SINUSOIDAL REACTION FORMULATION FOR RADIATION AND SCATTERING FROM CONDUCTING SURFACES

J. H. Richmond and N. Wang

The Ohio State University

ElectroScience Laboratory

Department of Electrical Engineering
Columbus, Ohio 43212

TECHNICAL REPORT 2902-11

January 1974

Grant Number NGL 36-008-138

National Aeronautics and Space Administration
Langley Research Center
Hampton, Va. 23365

NOTICES

When Government drawings, specifications, or other data are used for any purpose other than in connection with a definitely related Government procurement operation, the United States Government thereby incurs no responsibility nor any obligation whatsoever, and the fact that the Government may have formulated, furnished, or in any way supplied the said drawings, specifications, or other data, is not to be regarded by implication or otherwise as in any manner licensing the holder or any other person or corporation, or conveying any rights or permission to manufacture, use, or sell any patented invention that may in any way be related thereto.

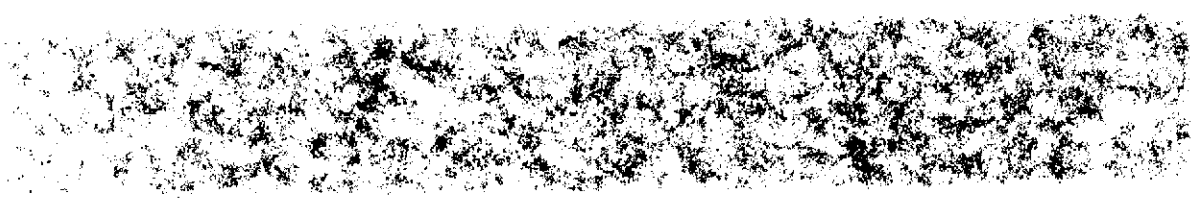

SINUSOIDAL REACTION FORMULATION FOR RADIATION AND SCATTERING FROM CONDUCTING SURFACES

J. H. Richmond and N. Wang

TECHNICAL REPORT 2902-11

January 1974

Grant Number NGL 36-008-138

National Aeronautics and Space Administration
Langley Research Center
Hampton, Va. 23365

ABSTRACT

A piecewise-sinusoidal reaction technique is developed for scattering and radiation from perfectly conducting bodies of arbitrary shape. This report presents the theory and numerical results for scattering patterns of rectangular plates and radiation patterns of corner-reflector antennas. In all cases, experimental measurements are included for comparison with the calculated data.

CONTENTS

I. INTRODUCTION

Electromagnetic boundary-value problems can be solved exactly via classical separation-of-variable analysis only for a few geometries, such as the sphere, spheroid, circular cylinder, elliptical cylinder, strip and wedge. Such solutions can be expressed in terms of a summation of a set of eigenfunctions which can be evaluated with a high speed computer. However, for problems involving complicated geometries the exact solution is not available. Thus, the approximate and numerical methods are of great significance. The research discussed herein is directed toward the numerical solution of the problems of radiation and scattering from conducting bodies of arbitrary shape.

Two methods are available for electromagnetic modeling of continuous conducting surfaces with arbitrary shape: the wire-grid model [1] and the surface-current model [2,3] using rectangular-pulse bases. Both methods have similar limitations with the maximum cell width restricted to approximately $\lambda/10$. Unless the conducting body is symmetric or is a figure of revolution, computer storage requirements have limited the moment-method application to bodies with surface area not exceeding one or two square wavelengths.

In this report, the piecewise-sinusoidal reaction technique applied by Richmond [4,5] to thin-wire antennas is extended to scattering by conducting bodies of arbitrary shape. The continuous conducting surface is divided into cells and the surface-current distribution is expanded in overlapping sinusoidal bases. Via an application of Galerkin's method, the integral equation formulated with the zero-reaction concept [6] is reduced to a matrix equation. From a physical viewpoint, this variational solution follows from enforcement of reaction tests with an array of sinusoidal electric test sources. The current distribution over the conducting surface is determined via matrix inversion. Finally the scattered field is obtained by integrating the surface currents.

The remaining text presents the detailed theory of the sinusoidal reaction formulation for radiation and scattering problems. The time dependence $e^{j\omega t}$ for the time-harmonic source is understood and suppressed. Numerical results are presented for the scattering patterns of rectangular plates and corner reflectors and the radiation patterns of corner-reflector antennas.

II. THE REACTION TECHNIQUE

The reaction concept and its applications have been discussed by Rumsey[6], Cohen[7], Harrington[8] and Richmond[9].

Consider the exterior scattering problem illustrated in Fig. 1a. In the presence of a dielectric or conducting body, the impressed electric and magnetic currents $(\underline{J}_i, \underline{M}_i)$ generate the electric and magnetic field intensities $(\underline{E}, \underline{H})$. For simplicity, let the exterior medium be free space.

From the surface-equivalence theorem of Schelkunoff[10], the interior field will vanish (without disturbing the exterior field) if we introduce the following surface-current densities

$$(1) \quad \underline{J}_s = \hat{n} \times \underline{H}$$

$$(2) \quad \underline{M}_s = \underline{E} \times \hat{n}$$

on the closed surface S of the scatterer. (The unit vector $\hat{n}$ is directed outward on S.) In this situation, illustrated in Fig. 1b, we may replace the scatterer with free space without disturbing the field anywhere.

By definition, the incident field $(\underline{E}_i, \underline{H}_i)$ is generated by $(\underline{J}_i, \underline{M}_i)$ in free space, and the scattered field is:

$$(3) \quad \underline{E}_s = \underline{E} - \underline{E}_i$$

$$(4) \quad \underline{H}_s = \underline{H} - \underline{H}_i \ .$$

When the surface current $(\underline{J}_s, \underline{M}_s)$ radiates in free space, it generates the field $(\underline{E}_s, \underline{H}_s)$ in the exterior and $(-\underline{E}_i, -\underline{H}_i)$ in the interior region. This result, illustrated in Fig. 1c, is deduced from Fig. 1b and the superposition theorem.

With the scatterer replaced by free space, we have noted in Fig. 1b that the interior region has a null field. As shown in Fig. 2, we place an electric test source $\underline{J}_t$ in this region and find from the reciprocity theorem that

$$(5) \quad \oint\!\!\!\oint_S (\underline{J}_s \cdot \underline{E}_t - \underline{M}_s \cdot \underline{H}_t)\, ds + \iiint (\underline{J}_i \cdot \underline{E}_t - \underline{M}_i \cdot \underline{H}_t)\, dv = 0$$

where $(\underline{E}_t, \underline{H}_t)$ is the free-space field of the test source. In words, Eq. (5) states that the interior test source has zero reaction with the other sources. This "zero-reaction theorem" was developed by Rumsey[6].

Equation (5) is the integral equation for the scattering problem, and our objective is to use this equation to determine the surface-current distributions $\underline{J}_s$ and $\underline{M}_s$. To accomplish this, we expand these functions in finite series so there will be a finite number N of unknown

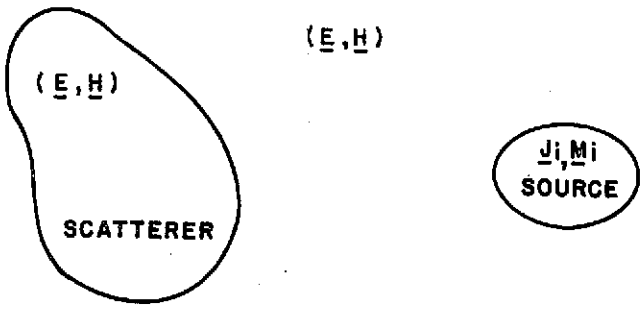

Fig. 1a. The source $(\underline{J}_i, \underline{M}_i)$ generates the field $(\underline{E}, \underline{H})$ with scatterer.

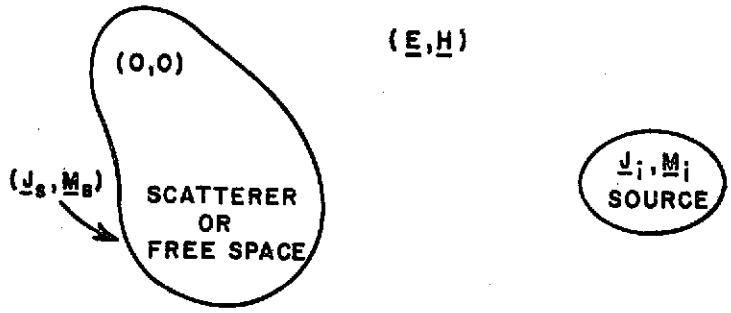

Fig. 1b. The interior field vanishes when the currents $(\underline{J}_S, \underline{M}_S)$ are introduced on the surface of the scatterer.

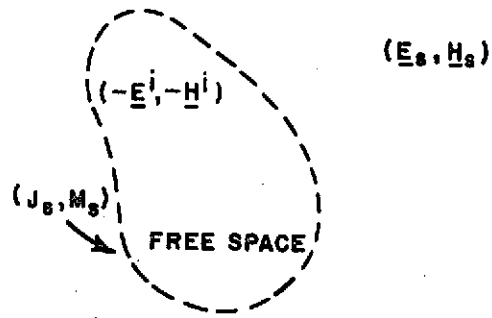

Fig. 1c. The exterior scattered field may be generated by $(\underline{J}_S, \underline{M}_S)$ in free space.

expansion constants. Next we obtain N simultaneous linear equations to permit a solution for these constants. One such equation is obtained from Eq. (5) each time we set up a new test source.

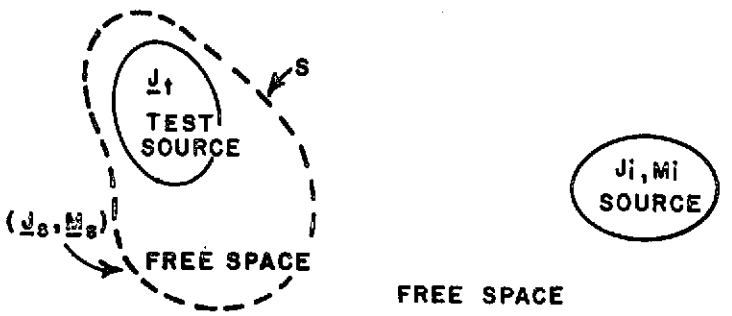

Fig. 2. An electric test source $\underline{J}_t$ is positioned in the interior of the scattering region.

The magnetic current $\underline{M}_S$ vanishes if the scatterer is a perfect conductor. We assume a finite conductivity and use the impedance boundary condition:

$$\underline{M}_S = Z_S \, \underline{J}_S \times \hat{n} \tag{6}$$

where Z_S denotes the surface impedance.

For 3-dimensional problems involving arbitrary scatterers, $\underline{J}_S$ and $\underline{M}_S$ are functions only of the position on the surface of the scatterer. If $\underline{M}_i$ vanishes, Eqs. (5) and (6) yield

$$-\iint_S \underline{J}_S \cdot [\underline{E}_m - (\hat{n} \times \underline{H}_m) Z_S] \, ds = \iint \underline{J}_i \cdot \underline{E}_m \, ds \tag{7}$$

where $(\underline{E}_m, \underline{H}_m)$ denotes the free-space field of test-source m.

We represent the electric current distribution as follows:

$$\underline{J}_S = \sum_{n=1}^{N} I_n \, \underline{J}_n \tag{8}$$

where the complex constants I_n are samples of the function J_S. The

vector functions $\underline{J}_n$ are known as basis functions, subsectional bases, expansion functions or dipole modes. We employ expansion functions $\underline{J}_n$ and test sources $\underline{J}_m$ with unit current density at the terminals.

From Eqs. (7) and (8) we obtain the simultaneous linear equations

$$(9) \qquad \sum_{n=1}^{N} I_n C_{mn} = A_m \quad \text{with } m = 1, 2, 3, \cdots N$$

where

$$(10) \qquad C_{mn} = -\iint_n \underline{J}_n \cdot [\underline{E}_m - (\hat{n} \times \underline{H}_m) Z_s] \, ds = -\iint_m \underline{J}_m \cdot \underline{E}_n \, ds$$

$$(11) \qquad A_m = \iint_i \underline{J}_i \cdot \underline{E}_m \, ds = \iint_m \underline{J}_m \cdot \underline{E}_i \, ds \, .$$

In Eqs. (10) and (11) the integrations extend over the region where the integrand is non-zero. For example, region n is that portion of the surface S covered by the expansion function $\underline{J}_n$. Region m covers the interior test source $\underline{J}_m$. The reciprocity theorem relates the first and second integrals in Eq. (10). In the second integral, $\underline{E}_n$ is the free-space field generated by $\underline{J}_n$ and the associated magnetic current $\underline{M}_n$.

For computational speed and storage, it will be advantageous to have a symmetric impedance matrix C_{mn}. Furthermore, the test sources should be selected to yield a well-conditioned set of simultaneous linear equations. For these reasons, we employ test sources $\underline{J}_m$ of the same size, shape and functional form as the expansion functions $\underline{J}_n$. Finally we position the interior test sources a small distance δ from surface S and take the limiting form of the integrals as δ tends to zero.

The next section discusses the electric surface dipoles which are employed as test sources and expansion modes.

III. THE SINUSOIDAL SURFACE DIPOLES

A planar surface dipole located on the yz plane is illustrated in Fig. 3a. This source is an electric surface-current density with height a and width b. The surface-current density is given by

$$\underline{J} = \hat{z} \cos\left(\frac{\pi(z-z_2)}{2(z_2-z_1)}\right) \quad \text{for } z_1 \leq z \leq z_2 \tag{12}$$

$$\underline{J} = \hat{z} \cos\left(\frac{\pi(z-z_2)}{2(z_3-z_2)}\right) \quad \text{for } z_2 \leq z \leq z_3 \tag{13}$$

As illustrated in Figs. 3b and 3c, the current density vanishes at the edges $z = z_1$ and $z = z_3$, and is uniformly distributed in the transverse direction. The surface-current density and its slope are continuous across the terminal at $z = z_2$.

The sinusoidal surface dipole is a hypothetical source in free space. The current distribution on a rectangular plate is not sinusoidal.

Figure 4 illustrates a surface V-dipole. Distance along the dipole arms is measured by the coordinates s and t with origin at the terminal 0. The surface-current density is

$$\underline{J} = -\hat{s} \cos\left(\frac{\pi s}{2s_1}\right) \quad \text{on arm s} \tag{14}$$

$$\underline{J} = \hat{t} \cos\left(\frac{\pi t}{2t_1}\right) \quad \text{on arm t.} \tag{15}$$

When the wedge angle ψ is adjusted to 180°, the V-dipole in Fig. 4 reduces to the planar dipole in Fig. 3a.

Having defined the sinusoidal surface dipole, one is now in a position to explain its relevance. The dipole current distribution (Eqs. (14) and (15)) will be used as the basis functions ($\underline{J}_n$ in Eq. (8)) for expanding the unknown current distribution induced on a conducting surface. Furthermore, surface dipoles will be employed as test sources with the reaction concept to solve the integral equation.

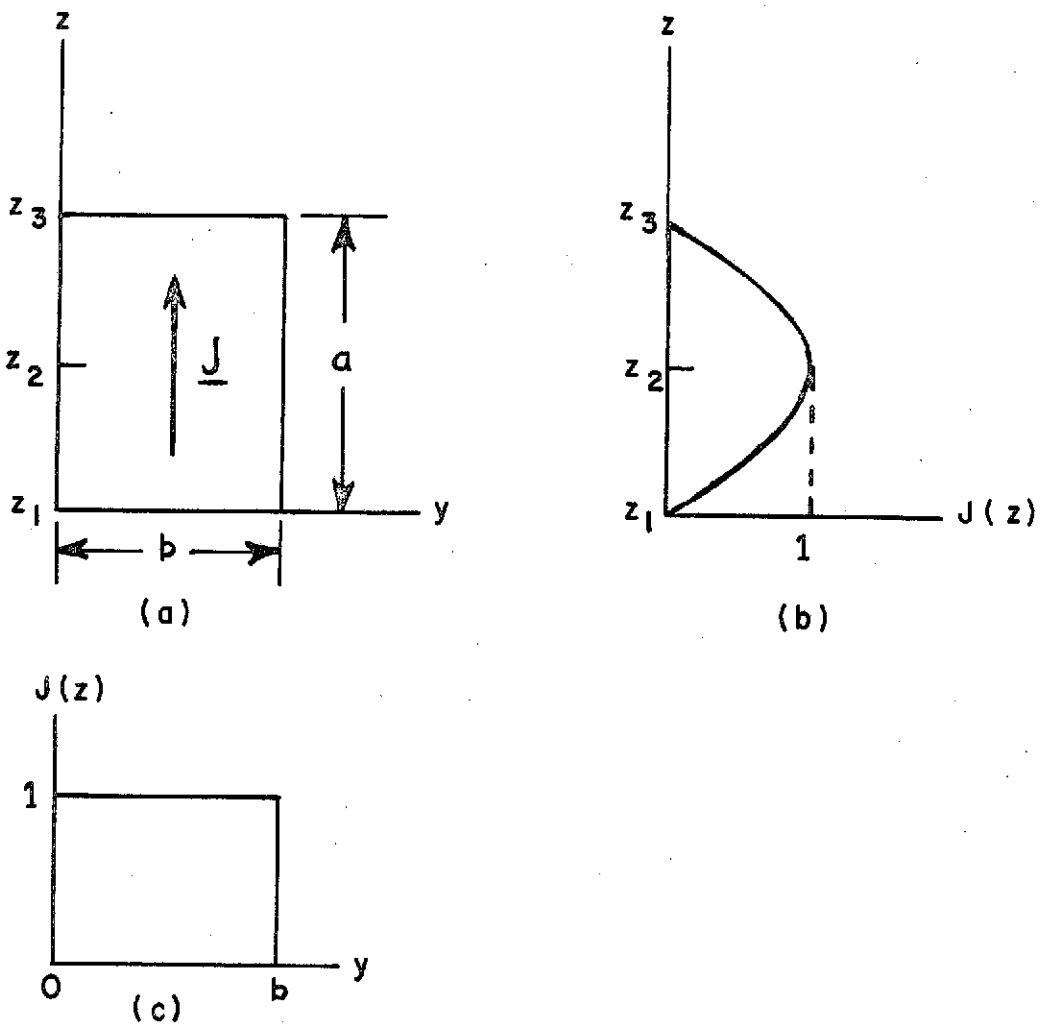

Fig. 3. An electric surface dipole and its current-density distribution.

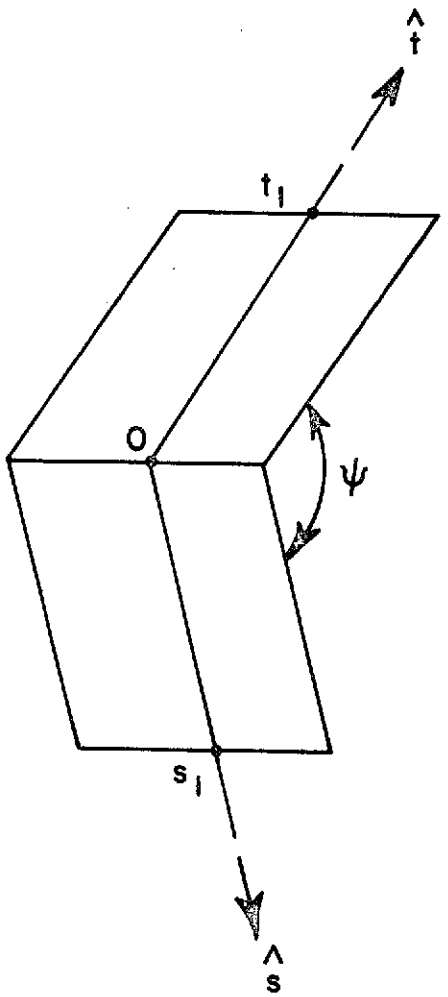

Fig. 4. A nonplanar surface dipole with edges at s_1 and t_1 and terminal at 0.

By superposition, the field of the surface dipole shown in Fig. 4 is the sum of the field contributions from monopoles s and t.

IV. THE IMPEDANCE MATRIX

From the viewpoint of reaction, the complex number C_{mn} in Eq. (10) represents the reaction between two sources. Let <m,n> denote the reaction between sources m and n, then Eq. (10) can be written as

$$C_{mn} = -\langle m,n \rangle = -\iint_m \underline{J}_m \cdot \underline{E}_n \, ds \, . \tag{16}$$

It has been pointed out [6] that the reaction between two sources is related to the circuit parameters by

$$C_{mn} = V_{mn} \, I_{mm} \tag{17}$$

where V_{mn} is the open circuit terminal voltage induced at m by source n, and I_{mm} is the terminal current of source m when it transmits.

Although the surface dipole described in Section III is a hypothetical source, it is useful to define its self-impedance with the induced-emf formulation:

$$Z_{mm} = \frac{V_{mm}}{I_{mm}} = \frac{C_{mm}}{I_{mm}^2} \, . \tag{18}$$

From Eq. (16), Eq. (18) yields

$$Z_{mm} = \frac{-1}{I_{mm}^2} \iint_m \underline{J}_m \cdot \underline{E}_m \, ds \tag{19}$$

where $\underline{J}_m$ is the surface-current density of source m and $\underline{E}_m$ is its free space electric field. The self-impedance of a center-fed, square surface dipole as a function of size is listed in Table I.

The mutual impedance between two surface dipoles is defined by

$$Z_{mn} = \frac{-1}{I_{mm} \, I_{nn}} \iint_m \underline{J}_m \cdot \underline{E}_n \, ds \, . \tag{20}$$

TABLE I

Self Impedance of Center-Fed Planar
Surface-Dipole Shown in Fig. 5

a/λ	R_{11}	X_{11}
0.2	11.48	-69.76
0.3	23.98	-35.26
0.4	38.80	-15.36
0.5	52.98	- 4.52

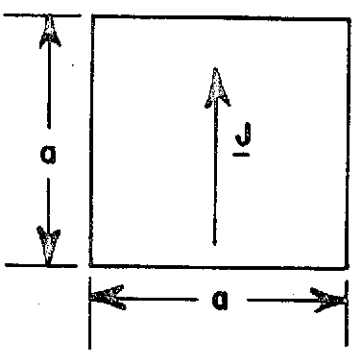

Fig. 5. Surface Dipole with $\underline{J} = \hat{z} \cos(\pi z/a)$

Figure 6 illustrates a pair of center-fed, coplanar surface dipoles, and Table II lists the mutual impedance Z_{12}. Here s_z and s_y specify the relative position of the dipoles.

V. THE EXCITATION COLUMN

The complex quantities A_m in Eq. (11) form the excitation column in the matrix equation $C_{mn}I_n = A_m$. Physically, A_m is the reaction between the impressed source and test dipole m. From Eq. (11), A_m is given by

$$A_m = \iint_m \underline{J}_m \cdot \underline{E}_i \, ds \, . \tag{21}$$

The above integral requires numerical integration over the source m. If the source $\underline{J}_i$ is located at a great distance from test dipole m, the incident field $(\underline{E}_i, \underline{H}_i)$ may be regarded as a plane wave with

$$\underline{E}_i = \underline{E}_o \, e^{jk(x'\sin\theta_i' \cos\phi_i' + y'\sin\theta_i' \sin\phi_i' + z'\cos\theta_i')} \tag{22}$$

where (r', θ_i', ϕ_i') are the spherical coordinates of the source and $\underline{E}_o$ is the incident electric field intensity at the coordinate origin O'. Figure 7 illustrates an incident plane wave illuminating an electric surface dipole located on the y'z' plane with height a and width b. For the surface-current density $\underline{J} = \hat{z}' \cos(\pi z'/a)$, Eq. (21) can readily be evaluated to yield

$$A_m = (\underline{E}_o \cdot \hat{z}') \, 2\pi ab \, \frac{\sin(X_i) \cos(Y_i/2)}{X_i (Y_i^2 - \pi^2)} \tag{23}$$

where

$$X_i = 0.5 \, kb \sin\theta_i' \sin\phi_i'$$

$$Y_i = ka \cos\theta_i' .$$

TABLE II
Mutual Impedance of Center-Fed Coplanar Surface Dipoles Shown in Fig. 6

$a/\lambda = 0.5$ $b/\lambda = 0.25$

0.75	1.076-j 7.913	-2.925-j 5.950	-5.968+j 1.761	0.8871+j 7.019
0.50	24.43 +j 5.997	10.04 -j 9.321	-9.568-j 6.65	-7.194 +j 8.971
0.25	53.10 +j55.87	29.54 -j 9.070	-9.468-j19.33	-15.74 +j 6.426
0.0	67.09 +j13.23	39.07 -j22.49	-8.659-j26.75	-19.32 +j 4.263
s_z/λ \ s_y/λ	0.0	0.25	0.50	0.75

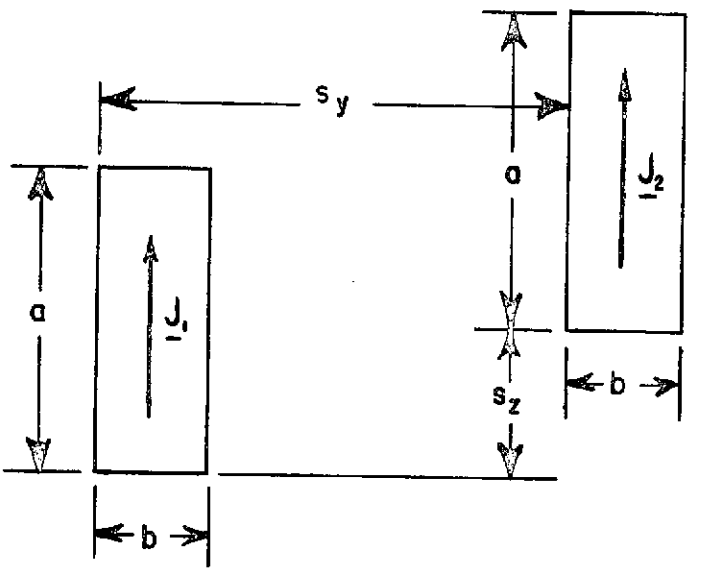

Fig. 6. Coupled surface dipoles

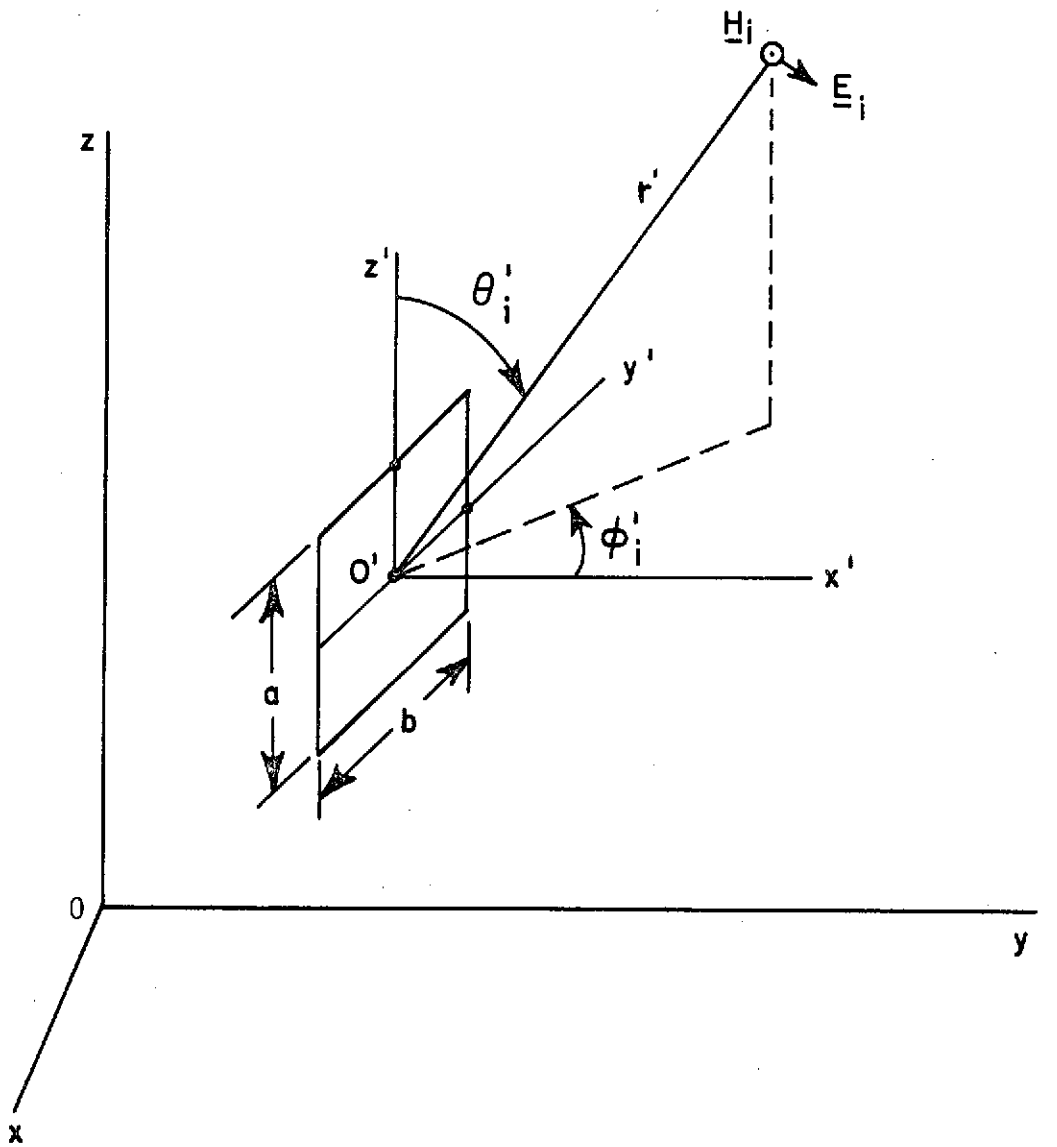

Fig. 7. A plane wave ($\underline{E}_i$,$\underline{H}_i$) illuminates an electric surface dipole.

VI. FAR-FIELD RADIATION AND SCATTERING

The field scattered by a perfectly conducting body may be generated by the electric surface-current density $\underline{J}_S$ in free space. To obtain the total field one adds the free-space field $(\underline{E}_i, \underline{H}_i)$ of the electric source $\underline{J}_i$.

Consider an electric surface dipole with current density $\underline{J}_S = \hat{z}' \cos(\pi z'/a)$ located on the y'z' plane as shown in Fig. 8. From reciprocity, the free-space electric field generated by this source at a distant point (r', θ_s', ϕ_s') is

$$\underline{E}^s = \hat{\theta}_s' \frac{j\omega\mu}{2} ab \frac{\sin(X_s)}{X_s} \frac{\cos(Y_s/2)}{(Y_s^2 - \pi^2)} \frac{e^{-jkr'}}{r'} \sin\theta_s' \tag{24}$$

where

$$X_s = 0.5\, kb \sin\theta_s' \sin\phi_s'$$

$$Y_s = ka \cos\theta_s' \,.$$

The $\hat{\theta}$- and $\hat{\phi}$-components of the scattered field with respect to the reference coordinate system 0 can be obtained easily via an appropriate coordinate transformation.

In plane-wave scattering problems, one is often interested in the echo area σ defined as follows

$$\sigma = \lim_{r\to\infty} 4\pi r^2 \frac{|\underline{E}^s|^2}{|\underline{E}^i|^2} \tag{25}$$

where $\underline{E}^i$ is the incident electric field intensity.

In antenna and radiation problems, one is interested in the power gain:

$$\text{Gain} = \frac{4\pi r^2 |\underline{E}|^2}{\eta |V|^2 G} \tag{26}$$

where V is the terminal voltage of the antenna, G is the terminal conductance of the antenna, and η is the intrinsic impedance of free space.

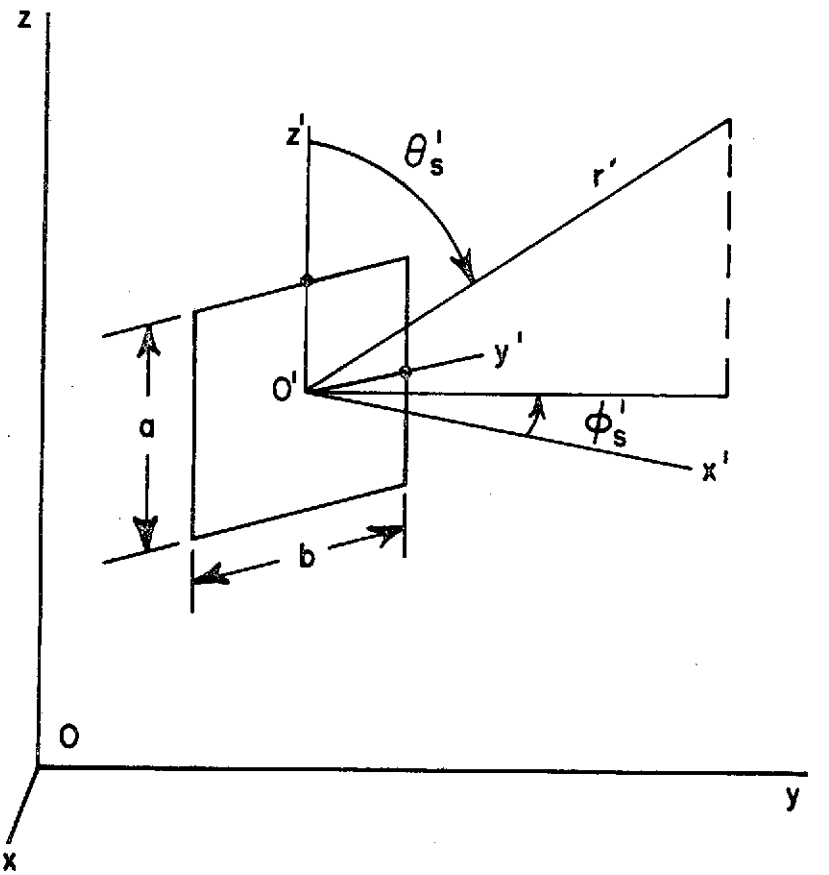

Fig. 8. A surface dipole radiates in free space.

VII. NUMERICAL RESULTS

Figure 9 presents the backscattering echo area of a square plate with perfect conductivity for the broadside aspect. In the reaction calculation, the plate is divided into cells, and overlapping current modes were employed as illustrated in Fig. 10. In this case the transverse current is neglected and 45 modes were used for the current distribution. Useful results can be obtained with as few as one mode per square wavelength of surface area. For comparison, Fig. 9 also shows the experimental measurements of Kouyoumjian [11].

The magnitude and phase of the current density induced on a perfectly-conducting rectangular plate are illustrated in Figs. 11 and 12. Figures 13 through 16 show the normalized backscatter cross-section of a rectangular plate. Figures 17 and 18 show the normalized backscatter cross-section of a corner reflector. The title of each figure gives the echo area at the broadside aspect in terms of dB = 10 log (σ/λ^2).

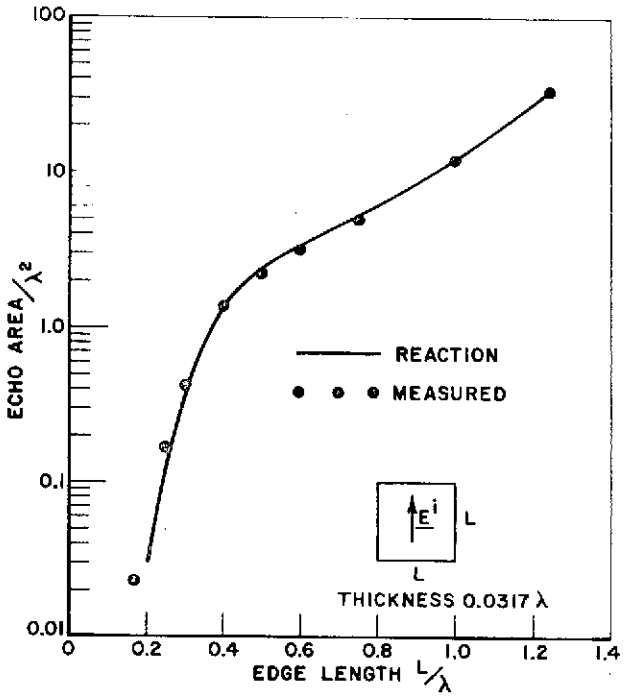

Fig. 9. Backscatter cross-section of perfectly conducting square plate for the broadside aspect.

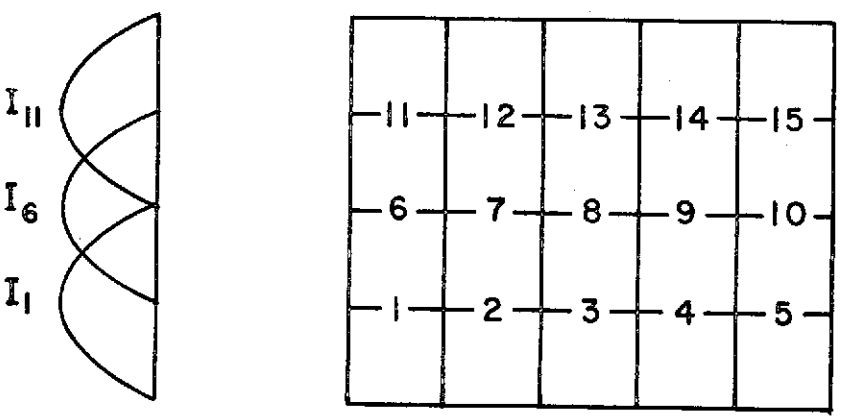

Fig. 10. Electromagnetic modeling of plate.

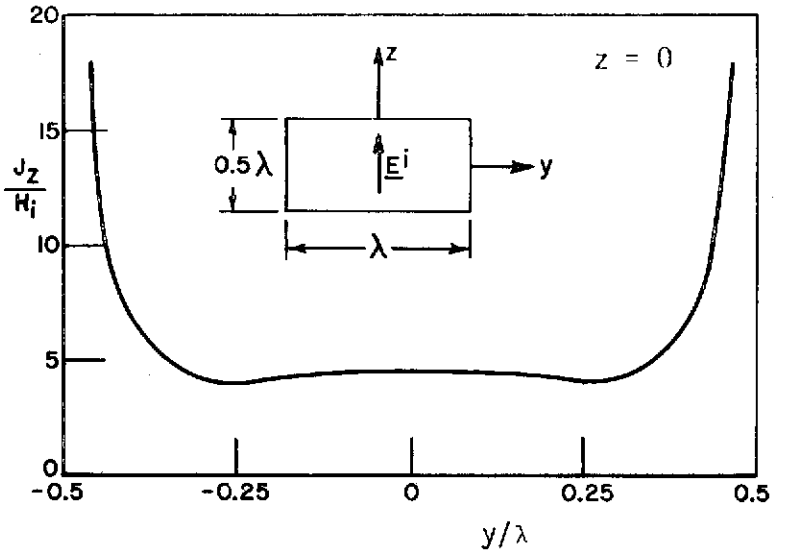

Fig. 11. Amplitude of surface-current density induced on a perfectly-conducting rectangular plate for a plane wave incident at broadside.

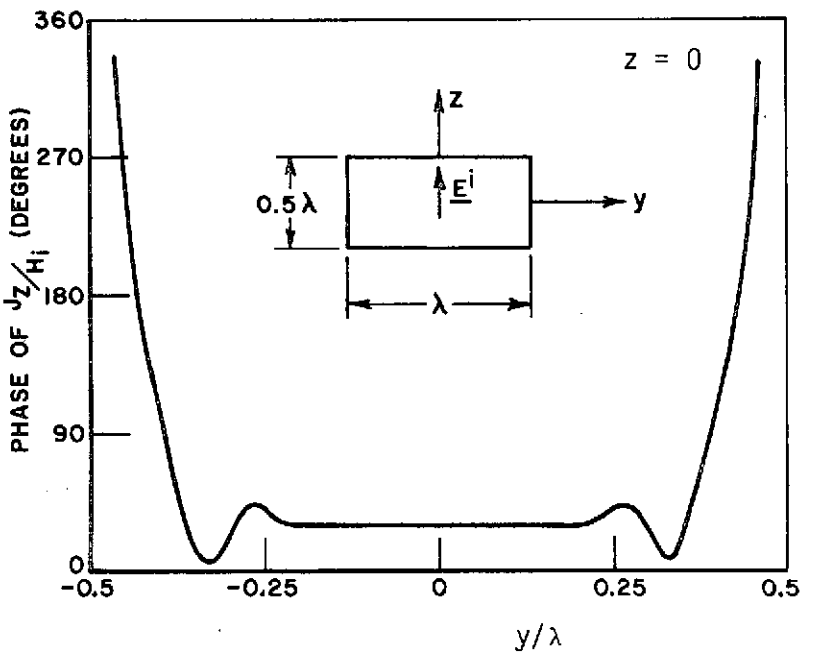

Fig. 12. Phase of surface-current density induced on a rectangular plate for a plane wave incident at broadside.

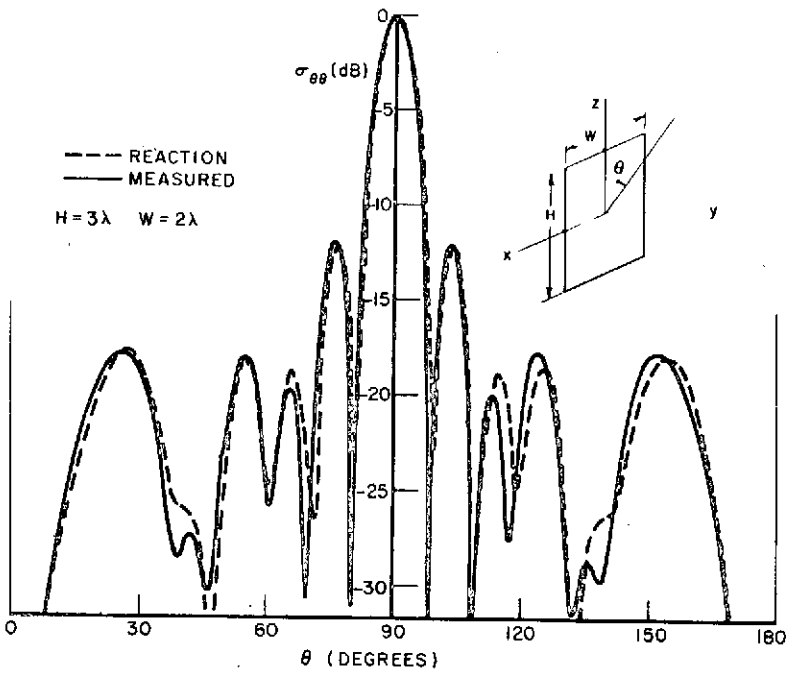

Fig. 13. Normalized backscatter cross-section in the yz plane of a rectangular plate. $\sigma_{\theta\theta}(\theta,\phi)$ = 15.25 dB at (90°,90°).

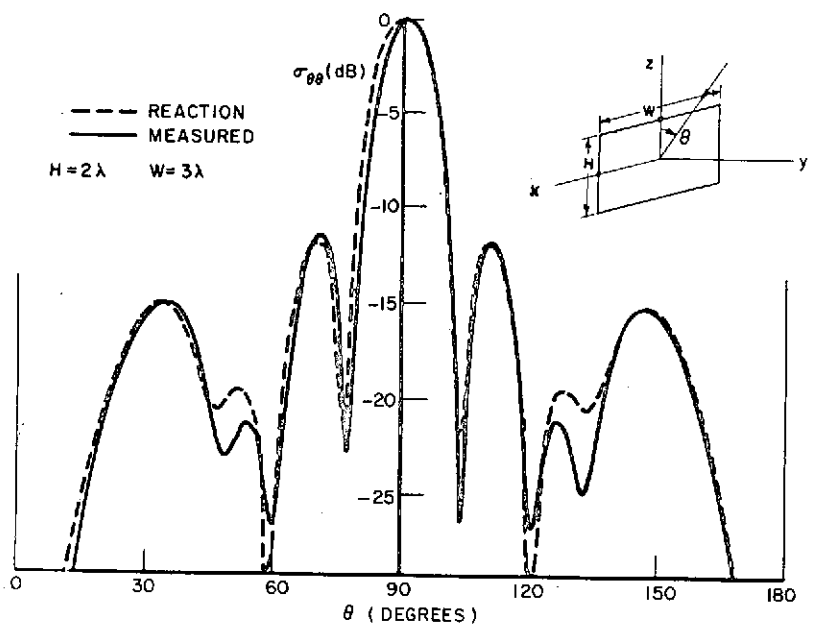

Fig. 14. Normalized backscatter cross-section in the yz plane of a rectangular plate. $\sigma_{\theta\theta}(\theta,\phi)$ = 15.23 dB at (90°,90°).

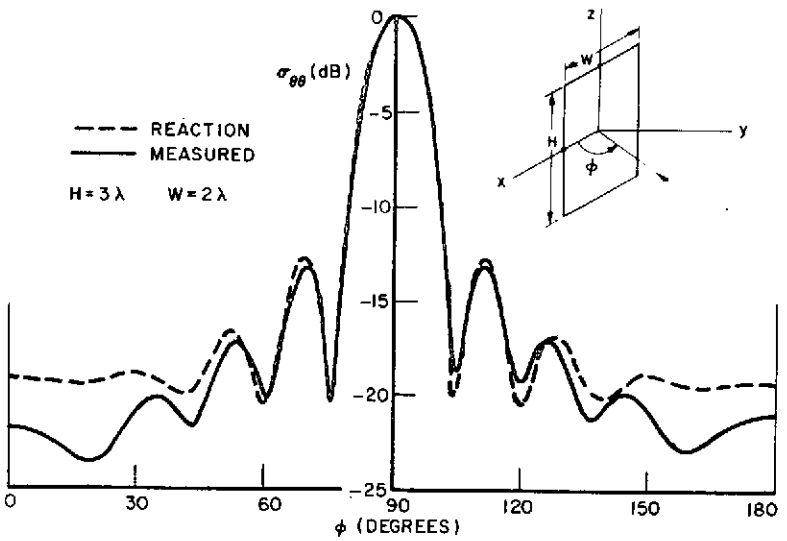

Fig. 15. Normalized backscatter cross-section in the xy plane of a rectangular plate. $\sigma_{\theta\theta}(\theta,\phi)$ = 15.25 dB at (90°,90°).

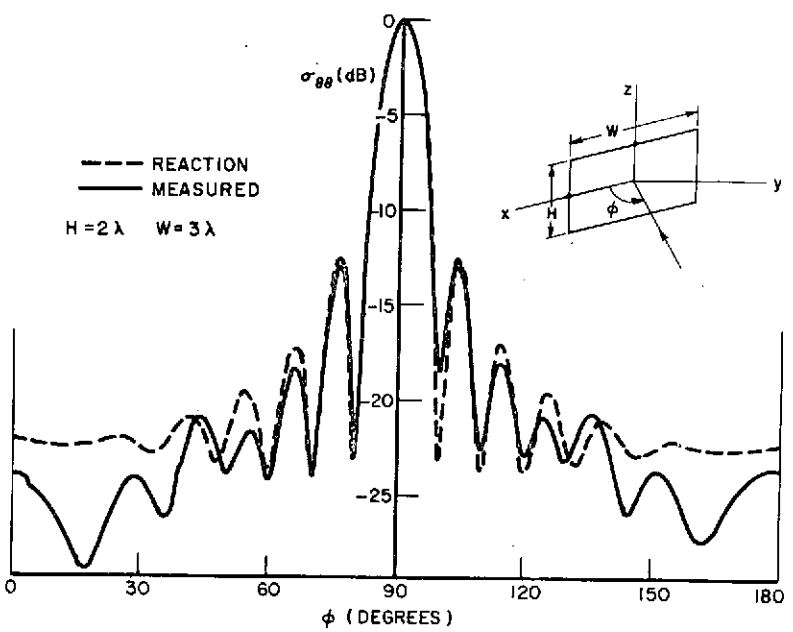

Fig. 16. Normalized backscatter cross-section in the xy plane of a rectangular plate. $\sigma_{\theta\theta}(\theta,\phi)$ = 15.23 dB at (90°,90°).

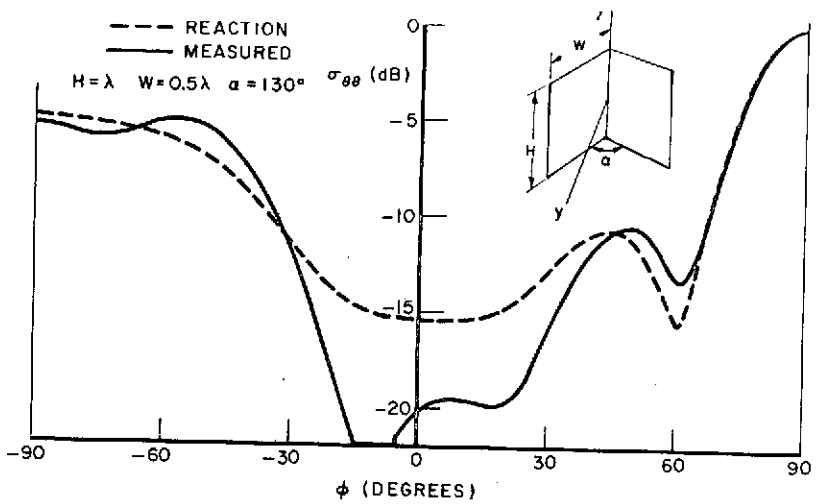

Fig. 17. Normalized backscatter cross-section in the xy plane of a corner reflector. $\sigma_{\theta\theta}(\theta,\phi)$ = -0.38 dB at (90°,90°).

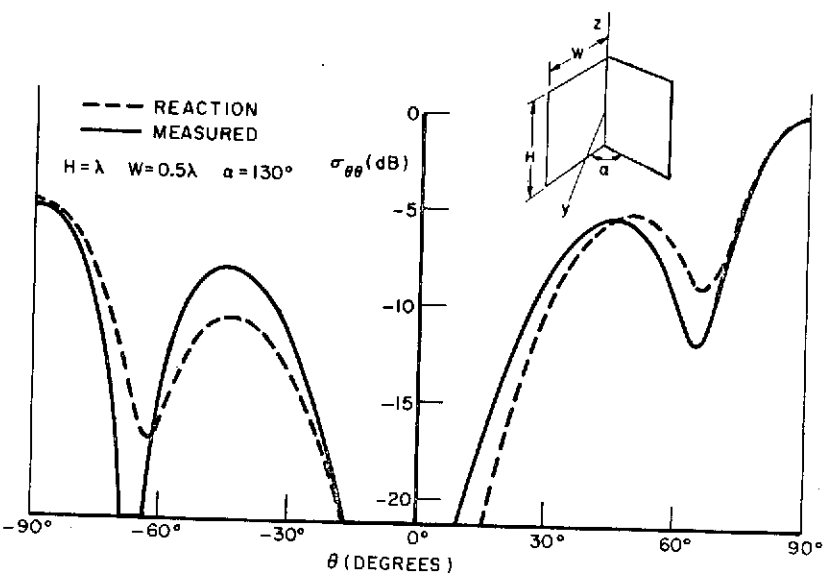

Fig. 18. Normalized backscatter cross-section in the yz plane of a corner reflector. $\sigma_{\theta\theta}(\theta,\phi)$ = - .38 dB at (90°,90°).

Figures 20 through 23 show the E-plane gain of the corner-reflector antenna illustrated in Fig. 19. Figures 24 through 27 show the H-plane gain of the same antenna. For comparison, Figs. 20 through 27 include experimental measurements obtained by Melvin Gilreath at NASA Langley Research Center. In the experimental measurements the receiving antenna was linearly polarized in the theta direction. Similarly, the calculated gain is based on E_θ. The dipole length is $\lambda/2$ and the radius is 0.005λ.

In the reaction calculation, only vertical modes were employed to approximate the current distribution. The number of modes used to obtain the results given in Figs. 11 through 27 are listed below. In each case, the matrix size is equal to the number of modes.

Figs.	Number of Modes
11,12	45
13,14	55
15,16	75
17,18	30
20-27	61

VIII. CONCLUSIONS

The reaction concept and Galerkin's method are used to develop a new formulation for perfectly-conducting antennas and scatterers. Numerical results are presented for scattering and radiation from rectangular plates and corner reflectors. The results show general agreement with measurements.

The techniques can be applied to surfaces with finite conductivity and arbitrary shape. For arbitrary polarization and aspect, 24 modes per square wavelength are adequate. This is a significant improvement over previous techniques.

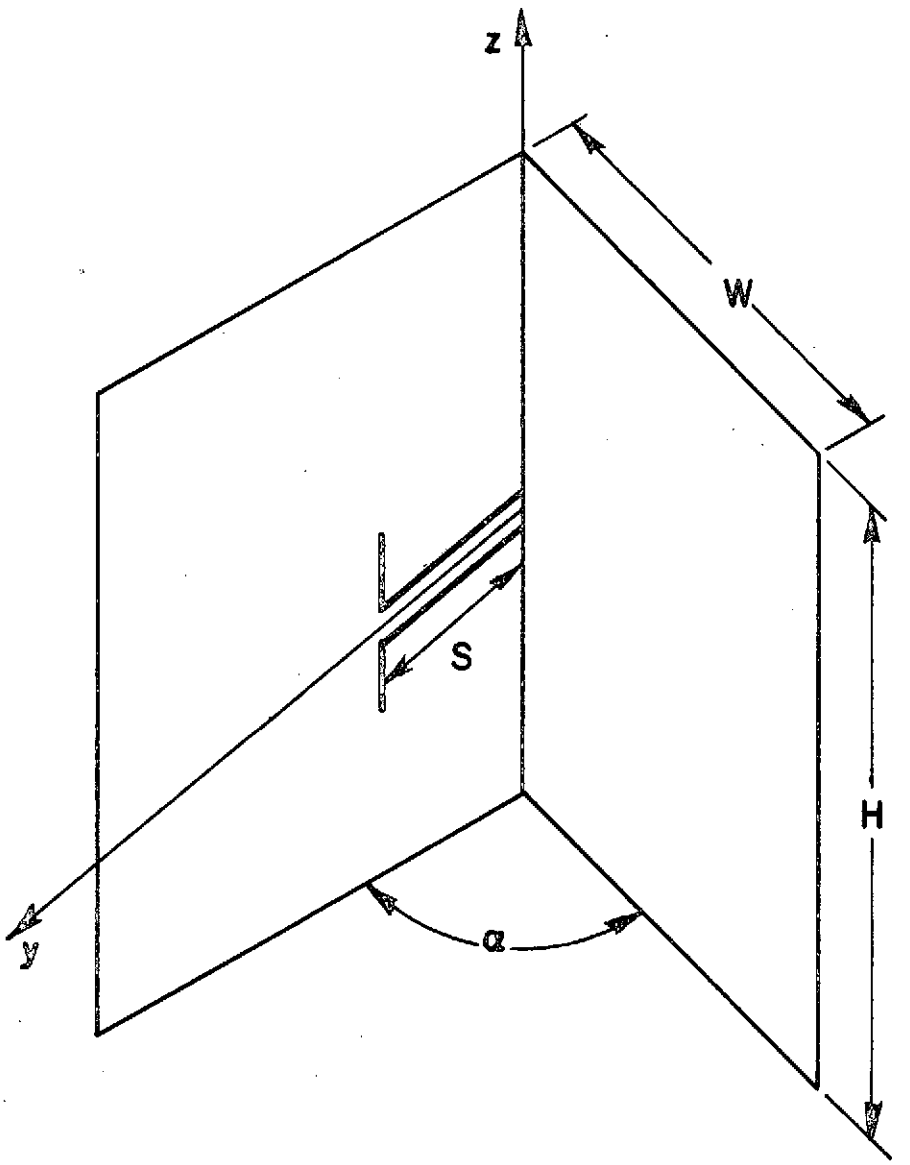

Fig. 19. Corner-reflector antenna.

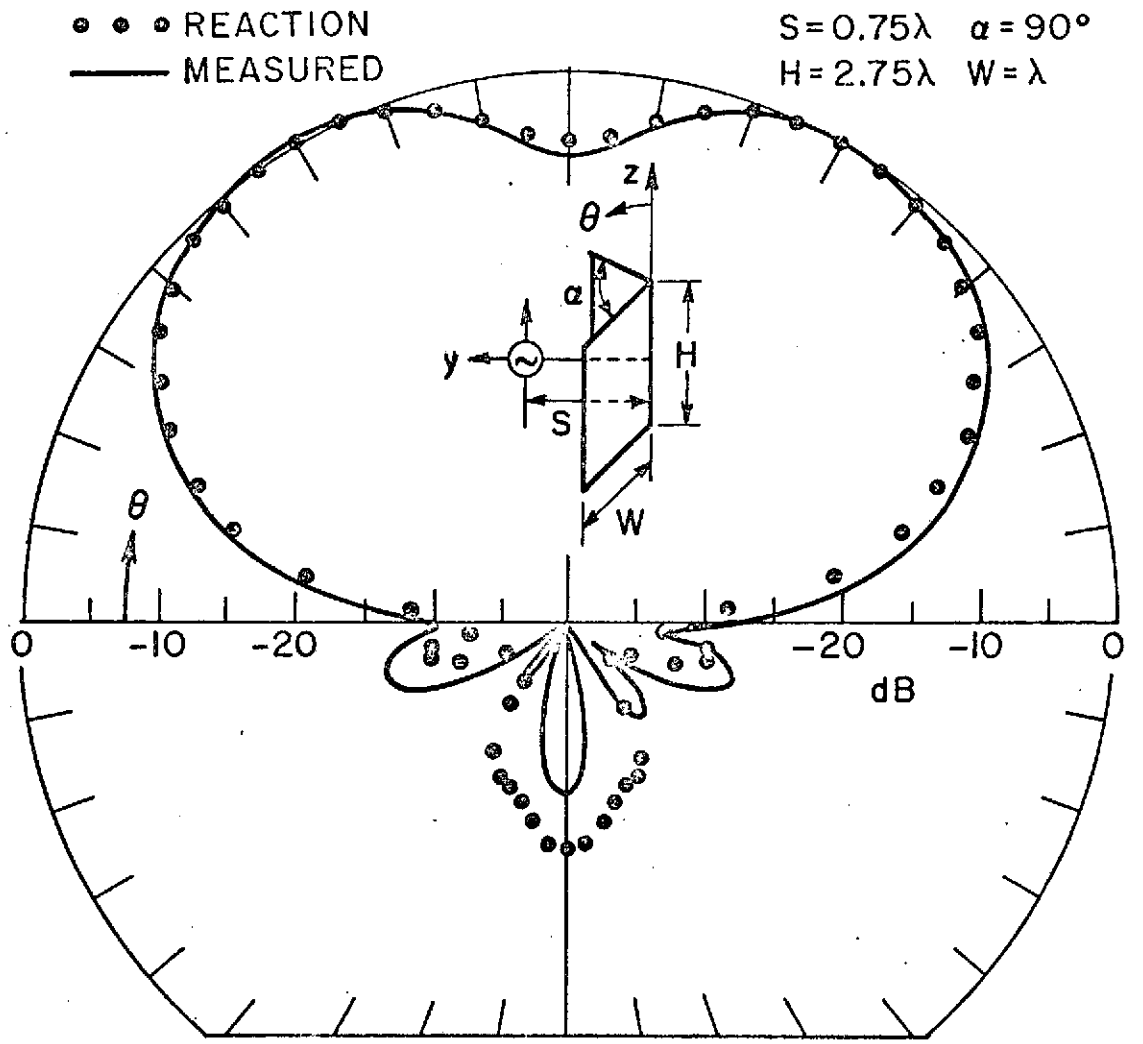

Fig. 20. Relative gain in the E-plane of a corner-reflector antenna. $G(\theta,\phi)$ = 4.31 dB at (90°,90°).

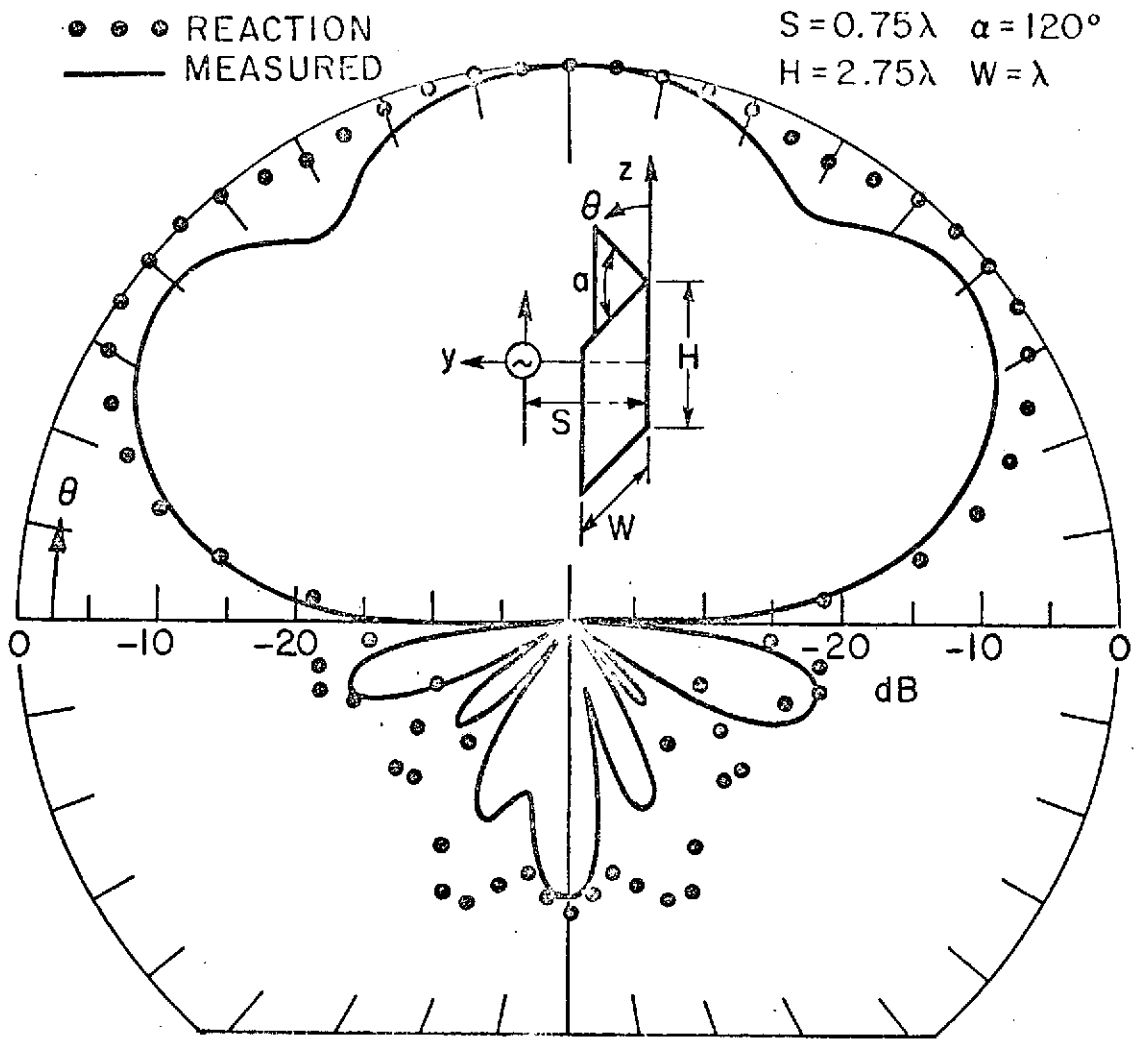

Fig. 21. Relative gain the the E-plane of a corner-reflector antenna. $G(\theta,\phi)$ = 4.05 dB at (90°,90°).

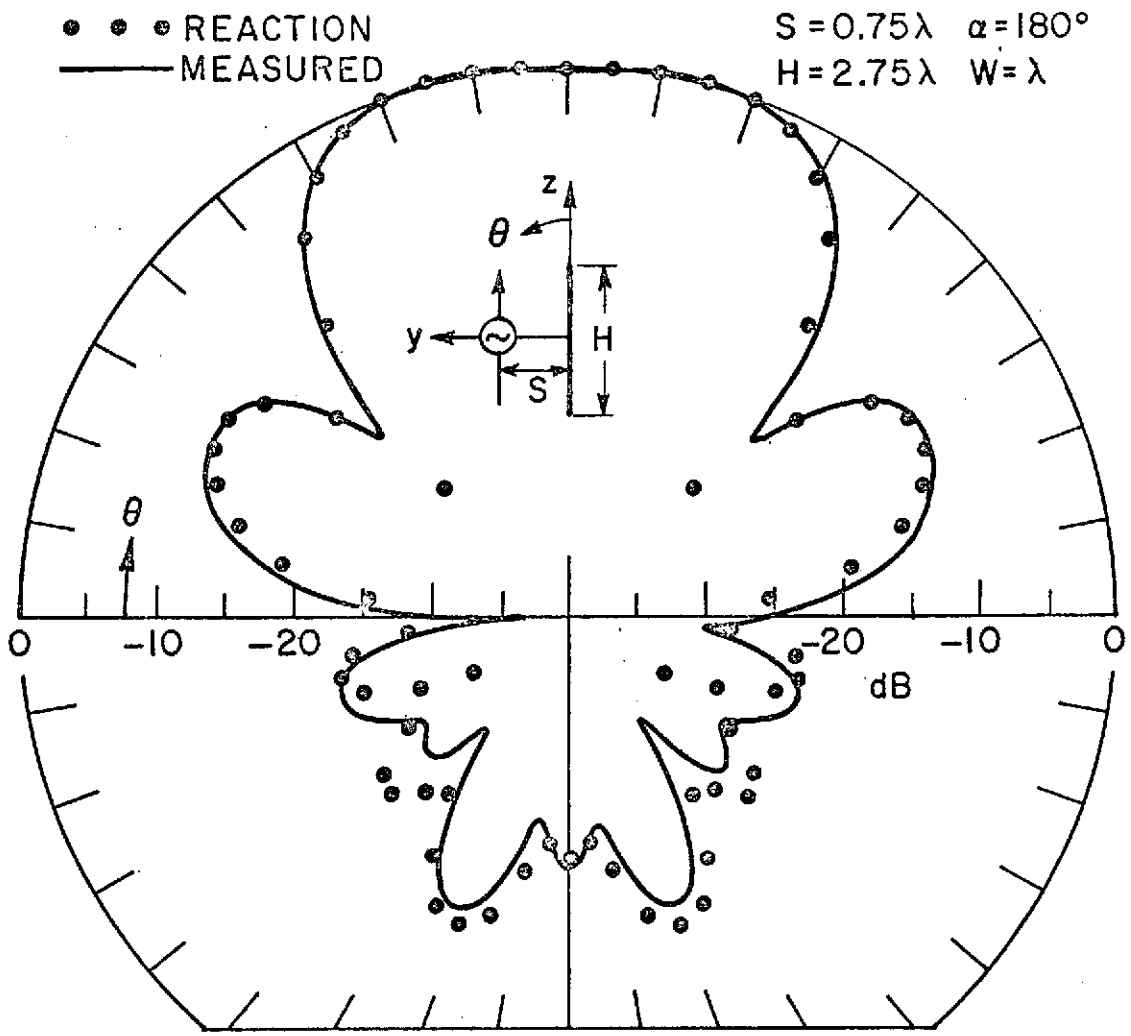

Fig. 22. Relative gain the the E-plane of a corner-reflector antenna. $G(\theta,\phi)$ = 7.48 dB at (90°,90°).

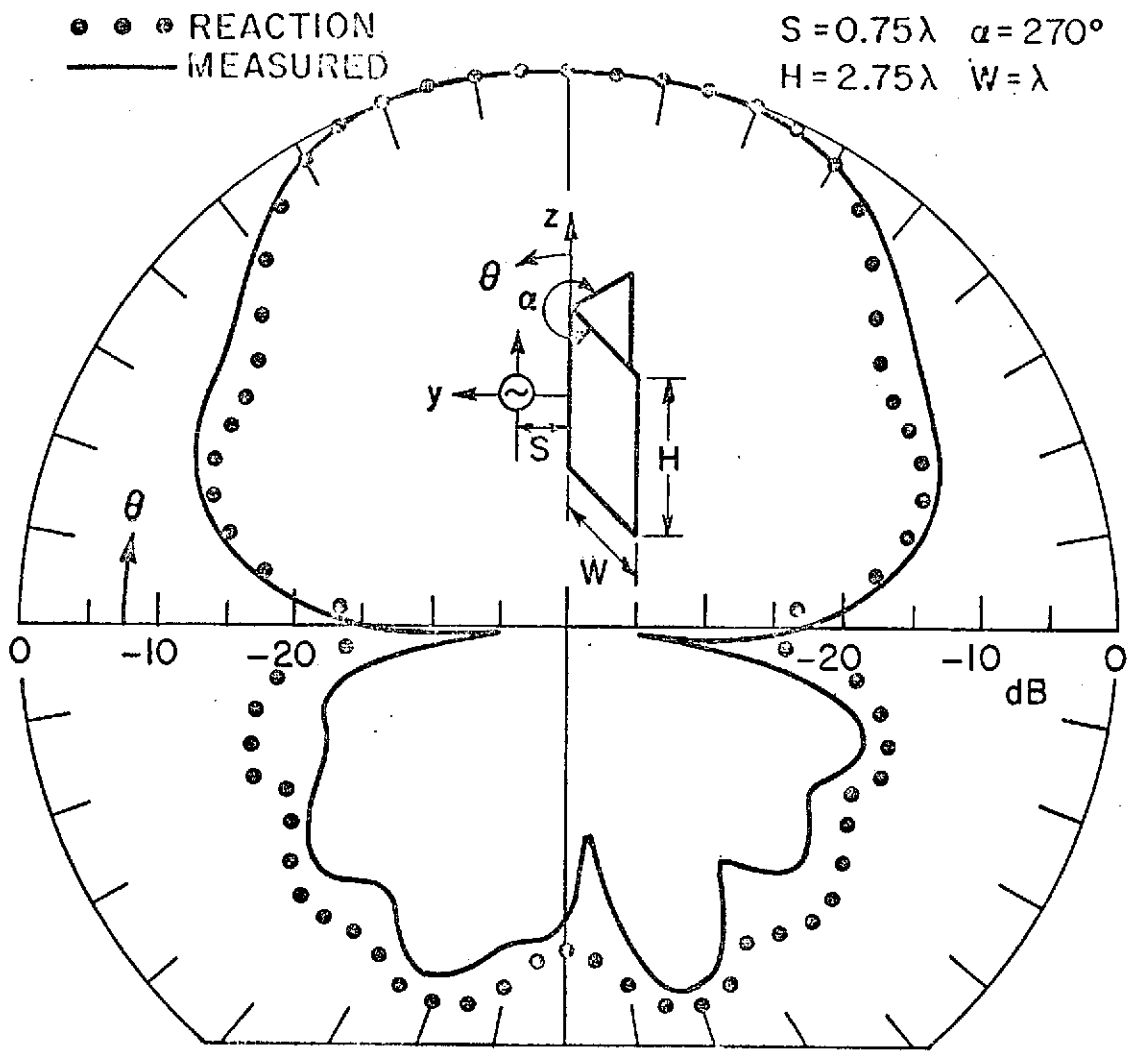

Fig. 23. Relative gain in the E-plane of a corner-reflector antenna. $G(\theta,\phi)$ = -1.06 dB at (90°,90°).

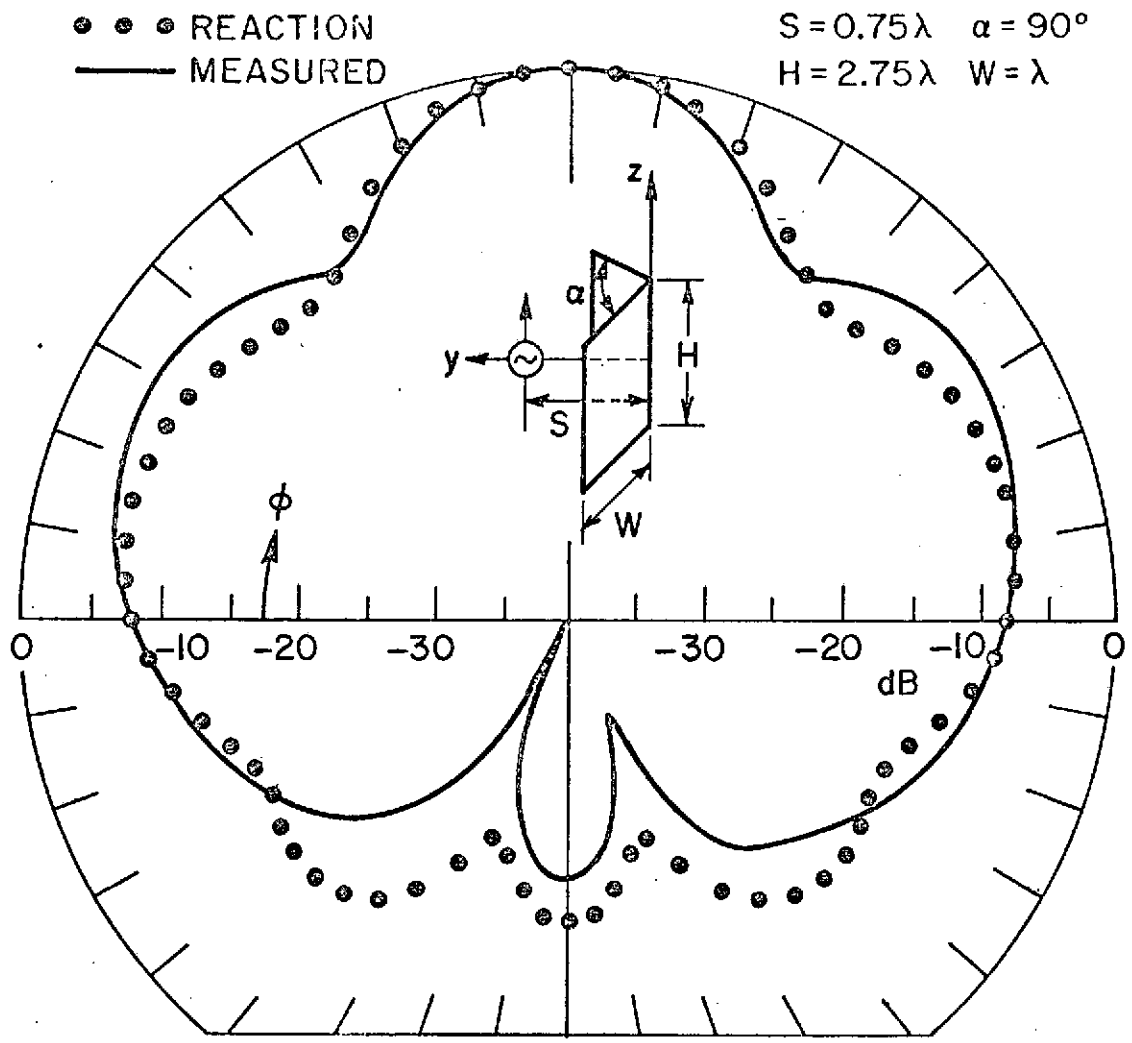

Fig. 24. Relative gain in the H-plane of a corner-reflector antenna. $G(\theta,\phi)$ = 4.31 dB at (90°,90°).

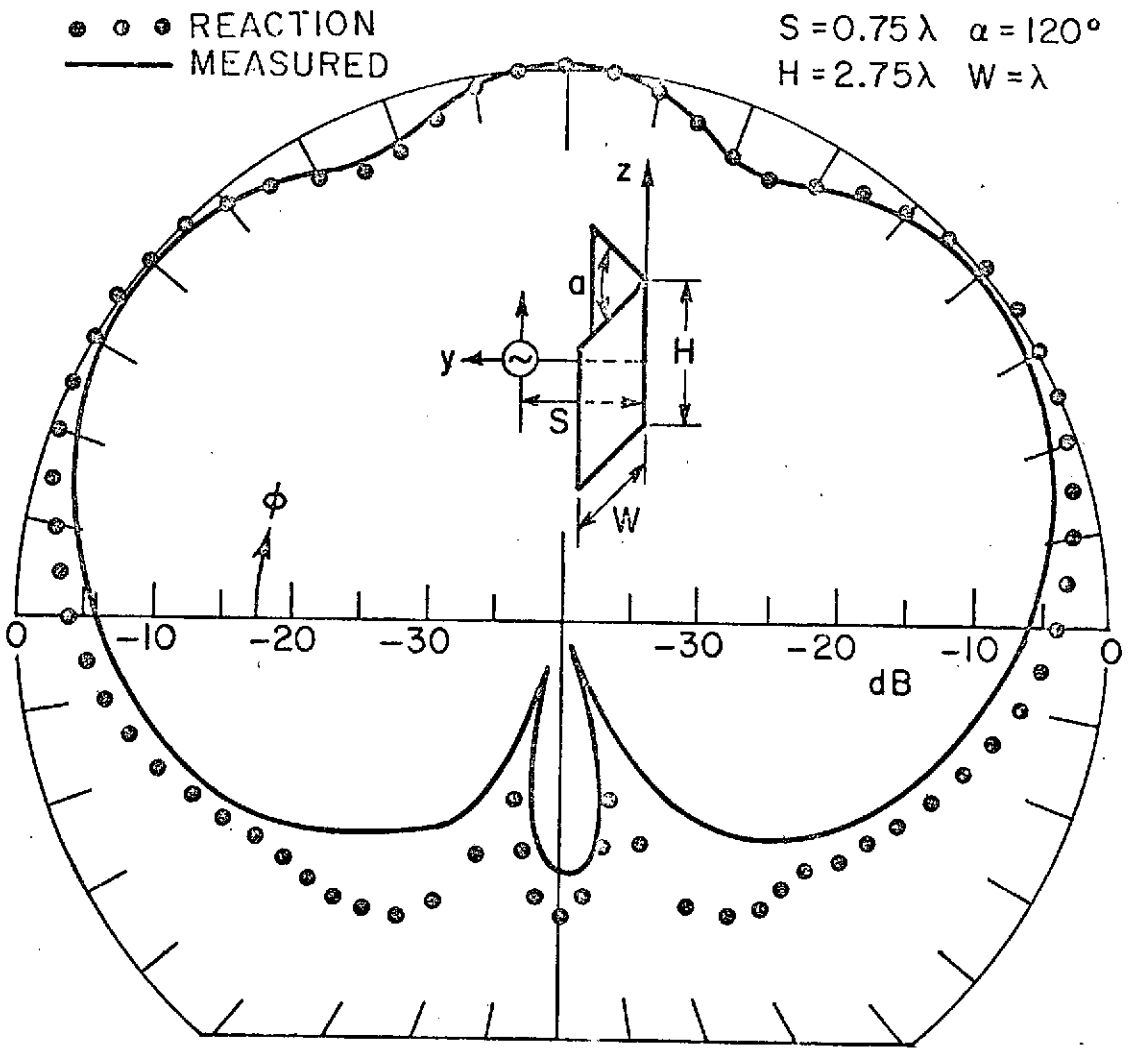

Fig. 25. Relative gain in the H-plane of a corner-reflector antenna. $G(\theta,\phi)$ = 4.05 dB at (90°,90°).

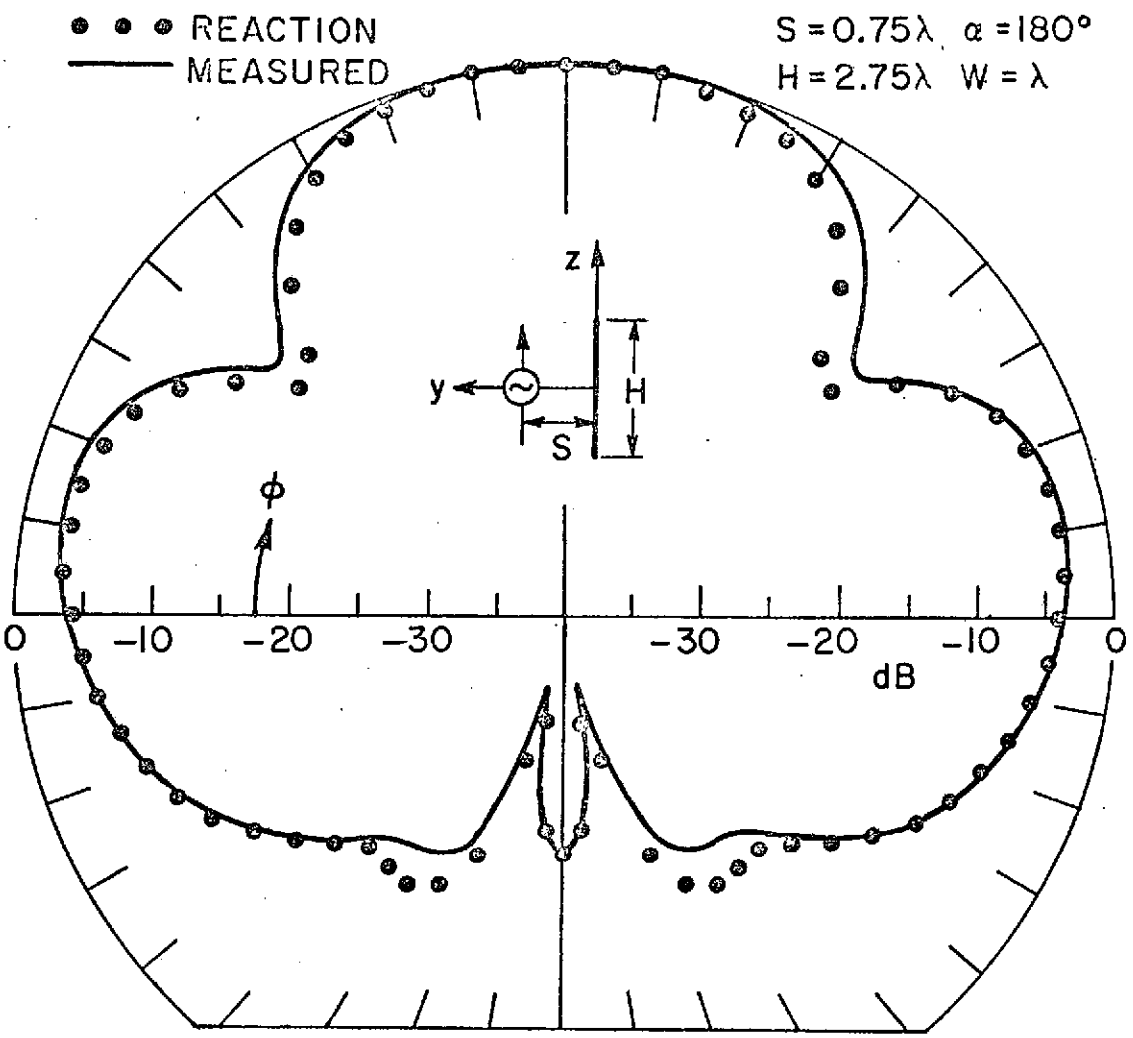

Fig. 26. Relative gain in the H-plane of a corner-reflector antenna. $G(\theta,\phi)$ = 7.48 dB at (90°,90°).

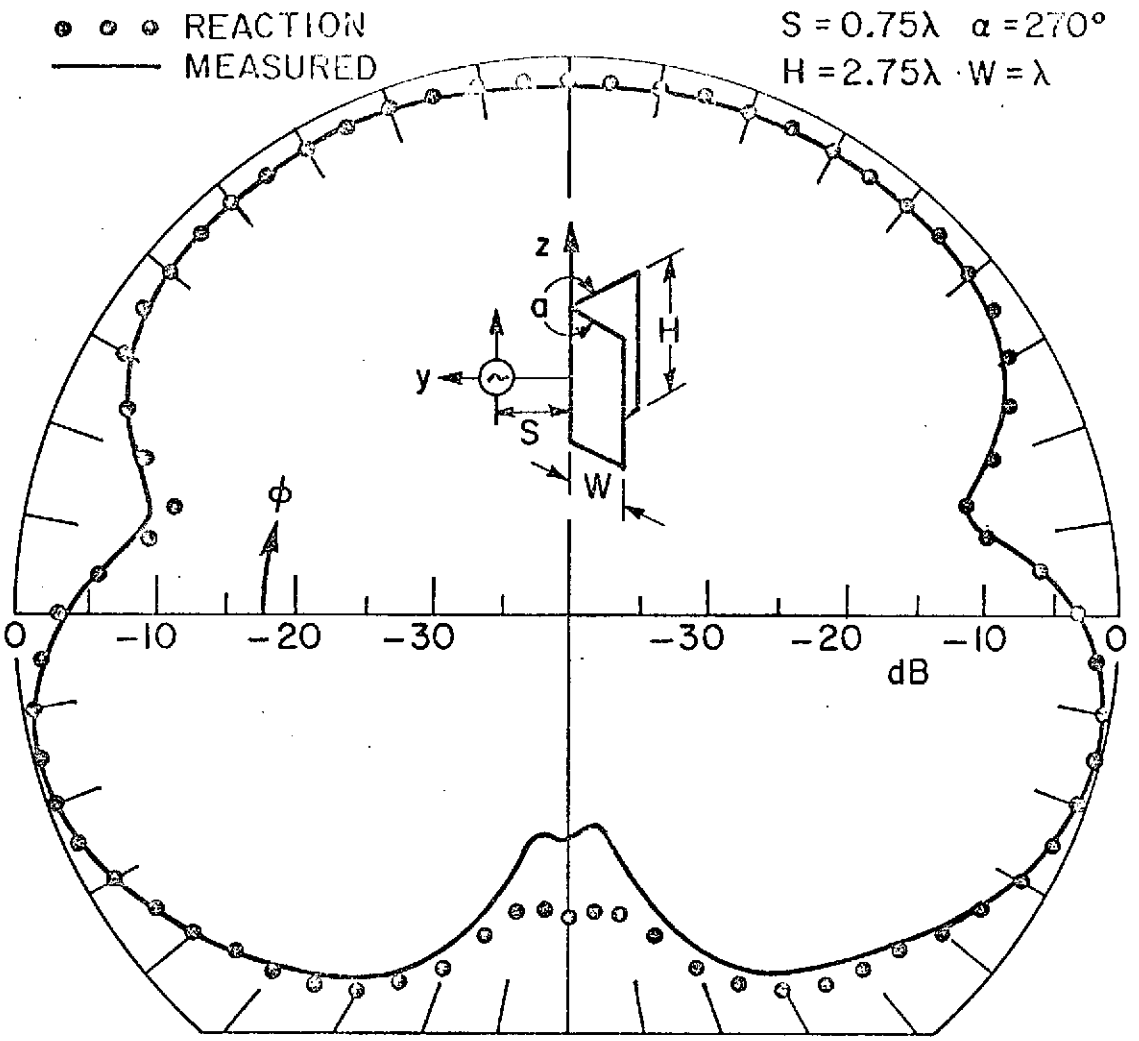

Fig. 27. Relative gain in the H-plane of a corner-reflector antenna. $G(\theta,\phi)$ = -1.06 dB at (90°,90°).

REFERENCES

[1] J. H. Richmond, "A Wire-Grid Model for Scattering by Conducting Bodies," IEEE Trans., Vol. AP-14, November 1966, pp. 782-786.

[2] F. K. Oshiro, "Source Distribution Technique for the Solution of General Electromagnetic Scattering Problems," Proc. First GISAT Symposium, Vol. 1, Part 1, Mitre Corporation, 1965.

[3] D. L. Knepp, "Numerical Analysis of Electromagnetic Radiation Properties of Smooth Conducting Bodies of Arbitrary Shape in the Presence of Known External Sources," Ph. D. Dissertation, University of Pennsylvania, 1971.

[4] J. H. Richmond, "Admittance Matrix of Coupled V Antennas," IEEE Trans., Vol. AP-18, November 1970, pp. 820-821.

[5] P. K. Agrawal, G. A. Richards, G. A. Thiele, and J. H. Richmond, "Analysis and Design of TEM-Line Antennas," IEEE Trans., Vol. AP-20, September 1972, pp. 561-568.

[6] V. H. Rumsey, "Reaction Concept in Electromagnetic Theory," Physical Review, Vol. 94, June 1954, pp. 1483-1491.

[7] M. H. Cohen, "Application of the Reaction Concept to Scattering Problems," IEEE Trans., Vol. AP-3, October 1955, pp. 193-199.

[8] R. F. Harrington, "Time-Harmonic Electromagnetic Fields," McGraw-Hill, New York, 1961, pp. 340-345.

[9] J. H. Richmond, "A Reaction Theorem and its Application to Antenna Impedance Calculation," IEEE Trans., Vol. AP-9, November 1961, pp. 515-520.

[10] S. A. Schelkunoff, "On Diffraction and Radiation of Electromagnetic Waves," Physical Review, Vol. 56, August 15, 1939.

[11] R. G. Kouyoumjian, "The Calculation of the Echo Area of Perfectly Conducting Objects by the Variational Method," Ph.D. Dissertation, The Ohio State University, 1953.

[12] J. H. Richmond, "Computer Analysis of Three-Dimensional Wire Antennas," Report 2708-4, 22 December 1969, The Ohio State University ElectroScience Laboratory, Department of Electrical Engineering; prepared under Contract DAAD05-69-C-0031 for Aberdeen Proving Ground, Maryland.

ACKNOWLEDGMENT

The experimental data on corner-reflector antennas were measured by Melvin C. Gilreath at NASA Langley Research Center. We appreciate sincerely his kind permission to reproduce these antenna patterns.